Multi-Objective Optimization of Kfloid-Type Gerotor Pumps for High-Pressure Applications

Harsh Kulkarni*, Andrea Vacca*, Jochen Hebel, Benjamin Ginsberg**, Christian Kretzer**, Matthias Krug****

Maha Fluid Power Center, Purdue University*

Thomas Magnete GmbH**

E-Mail:hkulkar@purdue.edu

Abstract.

Gerotor pumps have been successfully used in low pressure systems (< 50 bar) such as in automotive and in charge systems, owing to their low cost, low acoustic noise, and high filling capability. These positive features make gerotor still attractive in modern applications that require higher energy efficiency or reduced spatial claim. Therefore there is still an interest in studying alternative geometries with respect to the conventional ones. This paper takes into consideration a gerotor morphology referred to as Kfloid, which is not well studied in literature, and compare its performance with respect to a reference industry design. The approach of study is based on a parametric numerical optimization of this morphology, where the objective functions relate to specific displacement of the unit, sealing capabilities, flow non-uniformity and mechanical stress and wear. To allow such analysis, a numerical model for the generation and the processing of Kfloid profile is presented, and then used in an optimization workflow. Results include Pareto fronts highlighting trade-offs between the considered objective functions. To highlight the potential of the optimized Kfloid profile, comparison with a design previously optimized by the research team, and based on a cycloidal morphology are presented.

Keywords. Pumps, Gerotors, Optimization

1. INTRODUCTION

A gerotor gearset consists of an internally toothed gear and a conjugate externally toothed pinion of one tooth difference and features continuous contact between the rotors. The name was coined by its inventor by the combination of the two words "generated" and "rotor" [1]. Gaps between the teeth are sealed by the contact points and create control volumes that increase and decrease in size throughout a revolution, which enables a pumping action in the axial direction. An example of a typical gerotor pump is shown in Figure 1.

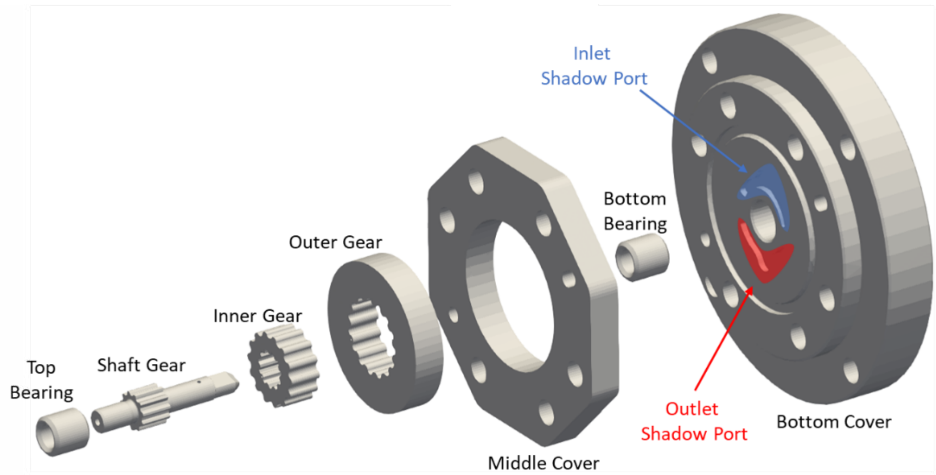

Figure 1: Typical Gerotor Assembly

Gerotor pumps are commonly employed in low-pressure applications such as oil, fuel, automatic transmission, and charge systems. They operate on a simple and elegant principle, requiring only a few components, which contributes to their robustness and cost-effectiveness. Their compact construction and suitability for powder metallurgy make them highly economical to manufacture. The most critical design consideration for a gerotor pump lies in the macro-geometry of its gears, as this directly influences the pump's displacement, flow ripple, efficiency, wear characteristics, and overall dimensions. Furthermore, the gears must maintain an appropriate drive relationship to ensure that the inner and outer rotors engage smoothly without the need for additional synchronization mechanisms.

In theory, for creating a gerotor profile any curve can be selected to form either the inner or outer gear, and a matching conjugate curve can be generated by applying the law of gearing [2]. An infinite number of possible profile families exist, each with an infinite number of profiles belonging to the family. This leads to the question, which is the best possible profile geometry? This is one of the main motivations behind undertaking this research for developing and understanding different profiles.

Much work has been done on multi-objective optimization of cycloidal gerotor profiles [5, 6, 12] and asymmetric profiles [11] has been done, but in these papers the main focus on the displacement, flow ripple and contact characteristics of the gerotor. The exploration of different composite profiles has been done by combining cycloidal and elliptical segments [13], cycloidal and circular arc curves [7], cycloidal and involute curves [8] and cycloidal curves with straight lines [3] has been conducted so far. But none of these works have tried to find an optimum pump geometry for high pressures at which the tip leakages become a very important consideration.

This work is motivated by the need to realize gerotor designs that operate reliably at higher pressures and speeds than conventional applications which in this study are considered to be 100 bars and 4000 RPM. A fast gear-generation algorithm is made and run within modeFRONTIER [16] to compute a Pareto set of candidate geometries. The paper first describes the gear-profile parameterization and generation procedure, then details the optimization framework in modeFRONTIER and the objective functions (OFs). The resulting designs are compared against an a few industry standard pumps that were available, and a subsequent stage of optimization is performed to refine the porting span for each Pareto-optimal geometry. The optimal design is selected from the Pareto front through additional analytical screening of candidate geometries, with primary emphasis on leakage performance. The best-performing design is then subjected to a lumped-parameter analysis to optimize the port geometry while accounting for operating pressure and speed.

2. Profile Description

The mixed profile named taken as reference in this work is the kfloid profile morphology illustrated in the work by Liu et al [3] where the author shows that the kfloid morphology performs better at higher pressure in terms of volumetric efficiency. A kfloid half-tooth section can be very simply defined by three sections which are two shifted cycloidal sections connected by a straight line of length L which is by definition a common tangent to the two end points of the shifted cycloids as shown in figure 2.

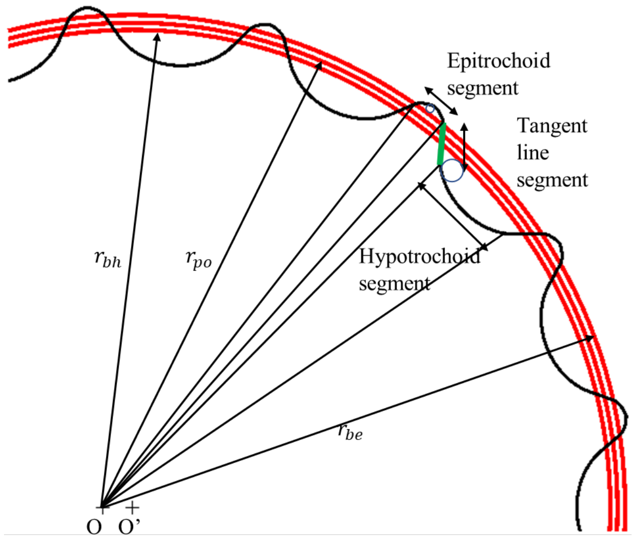

Figure 2: Geometric definition of quantities in a Kfloid profile, adapted from [3]

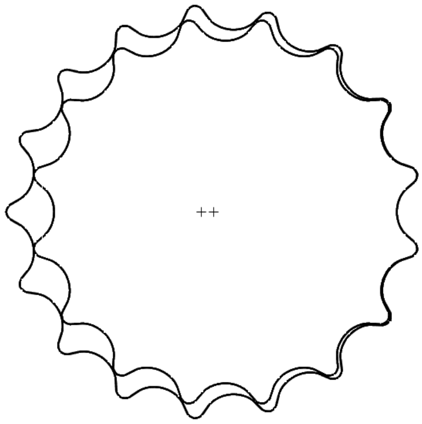

Figure 3: Example of a Kfloid gearset

The parametrization of the profile is done with the sets of uniquely defined parameters mentioned in table 1. This parametrization can be used to define either of the inner or outer gears.

In theory with the application of the law of gearing the generated Kfloid gear can be considered an inner or outer gear, but in this study the generated gear is defined as the outer gear and using the law of gearing the inner gear is generated from the defined outer gear. A resulting Kfloid inner and outer gearset is shown below in figure 3.

Parameter	**Value**	**Unit**
Number of Teeth	17	-
Eccentricity	3.190	mm
d	2.241	mm
b	1.344	mm
r_{po}	54.230	mm
s_{hypo}	0.848	mm
s_{epi}	5.231	mm
$\Delta\theta_1$.	315.573	deg
$\Delta\theta_2$.	287.965	deg

Table 1: Parametrization used to uniquely define the Kfloid gear in figure 3.

3. GEOMETRY CODE

The geometry code implements a numerical procedure for discretizing the pump domain into displacement chambers (DCs) by identifying minimum-distance segments between the inner and outer rotors that uniquely bound each chamber and preserve continuity of the enclosed fluid volume over a full revolution. This method is based on the approach of Pelligri et al. [14], with targeted modifications to achieve smoother chamber evolution in the vicinity of the dead-volume region. In particular, the minimum-gap criterion is selectively deactivated over a small angular interval, and the DC boundaries are interpolated to provide a continuous and physically consistent transition through this region. The parameters extracted from the geometry code are summarized in Table 2, while Figures 5(a) and 5(b) illustrate the evolution of the DC near the dead volume at shaft angles of 320° and 340°, where the modified interpolation procedure replaces the standard minimum-distance algorithm to ensure a smoother transition.

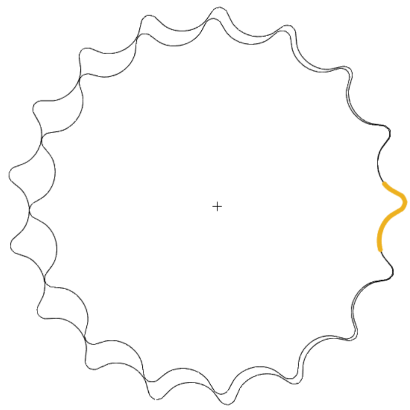

Figure 5 (a): DC definition at an angle of 320° of the outer rotor rotation

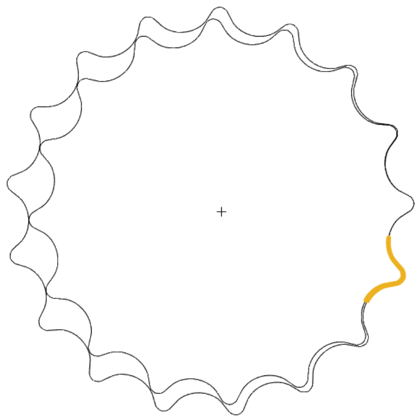

Figure 5 (b): DC definition at an angle of 340° of the outer rotor rotation

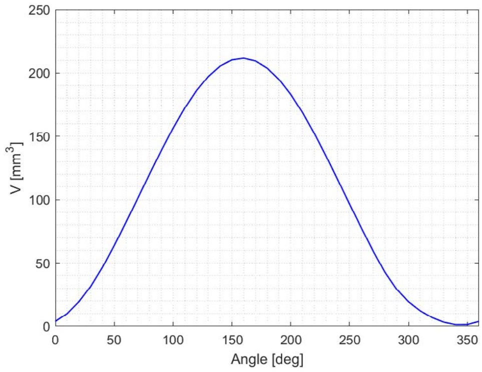

Figure 6: Resulting volume variation with the variation in outer rotor shaft angle

Parameter	Description
V	Displacement Chamber Volume (DCV) [mm^3]
h_t	Clearance gap height [mm]
Ω	DCV projected area [mm^2]
$\frac{dV}{d\theta}$	Rate of change of volume w.r.t rotation [mm^3/deg]
R_{eq}	Equivalent radius of curvature at contact point [mm]
$\hat{n}$	Contact point normal vector
v_x	Contact point velocity [m/s]

Table 2: Parameters obtained from the numerical geometry code

4. OPTIMIZATION METHODOLOGY

The gear generation and optimization framework uses the MOGA-II algorithm [17], which was selected for its suitability in handling multi-objective optimization problems through Pareto-based ranking rather than objective scalarization. This approach provides a broader understanding of the trade-offs between design parameters and helps identify an optimal family of solutions rather than a single design point. The first step of the design optimization was executed for a total of 350 generations, with the initial Design of Experiments (DOE) populated using a constraint-satisfaction sampling method to ensure that only geometrically feasible configurations were evaluated, the DOE table was populated by 100 designs in total. A numerical algorithm is used to numerically discretize the pump domain into isolated displacement chambers by drawing segments along the regions of minimum gap height, allowing for continuous variation in the computed chamber volume V(θ) along with other geometric properties of interest such as the tooth-tip gap height, the projected areas of the DCs and the curvatures of the gears in contact of the DC throughout the rotation for different rotational orientations.

Input Parameter	Min. Value	Max. Value	Unit
Number of Teeth	5	20	-
Eccentricity	0.5	5	mm
d	0.5	4.5	mm
b	0.5	4.5	mm
r_{po}	2.5	100.0	mm
s_{hypo}	0.0	10.0	mm
s_{epi}	0.0	10.0	mm
$\Delta\theta_1$.	300.0	420.0	deg
$\Delta\theta_2$.	240.0	330.0	deg

Table 3: Limits of variation of each geometric input parameter for the optimization

Parameter	Constraint	Value	Unit
Gear Root Radius	Lesser than	45	mm
Connecting Segment Length	Greater than	0	mm
Gear Intersection Area	Lesser than or equal to	0	mm^2
Minimum Chamber Volume	Equal to	10^{-9}	mm^3

Table 4: Constraints applied to each generated gear design for the analytical optimization

The algorithm selects geometric parameters which are described in table 3 within the prescribed design space and scales the pump dimensions to achieve the specified displacement of 3.365 cc/rev, which is maintained constant across all configurations for consistent comparison. The variables in table 3 describes the rolling circle parameters for the inner and outer cycloids namely as the rolling circle radius, base circle shift and angle of rotation for the inner circle as b, s_{hypo}, and $\Delta\theta_1$ as well as the outer circle parameters d, s_{epi}, and $\Delta\theta_2$ and the outer rotor root circle radius is r_{po}. Additional constraints are imposed on the maximum allowable radius and leakage rate to prevent unrealistic or non-physical designs in the analytical optimization along with a minimum chamber volume, these constrains are described in table 4. The optimization proceeds in two stages which are described in more detail further in section 4. The first stage involves analytical screening and ranking of designs based on leakage and stress performance described in the objective functions in section 4.1, while the second stage refines the selected candidate designs using a lumped-parameter simulation of the porting system to maximize both volumetric and hydromechanical efficiencies. Designs violating any geometric constraints described in table 4 are automatically discarded, and the MOGA-II evolutionary operators iteratively evolve the feasible population toward the Pareto-optimal front. This framework is flexible and can accommodate additional objective functions such as minimizing wear or stress concentrations within the same multi-objective optimization procedure as described later in section 4.

5. OBJECTIVE FUNCTIONS

5.1. *Analytical Design optimization*

The objective of this optimization is to analytically identify the top-ranked gerotor designs with minimal leakage, so they can be selected from the Pareto front and advanced to the second optimization stage. Figure 7 gives a good overview of the complete optimization procedure. The feasibility of the geometry is obtained based on the constraints in table 4 and the design evaluation is performed by the numerical geometry code which extracts the parameters listed in table 2 in order to calculate the objective functions.

5.1.1. *Gerotor sizing*

$$OF1\colon minimize\ r_o \tag{4.1}$$

For this project the expected delivery flow from the gerotor was fixed as per the requirements of the sponsor along with the width of the pump, a scaling algorithm for the gear radius was applied to ensure that the gerotor displacement is within the specification while the radius of the pump outer rotor r_o is minimized as per the objective function given in equation (4.1) and additionally a constraint on the outer radius was applied to ensure the sizing limits of the pump. The radius is defined as the distance of the farthest point on the outer rotor from the centre of the outer rotor.

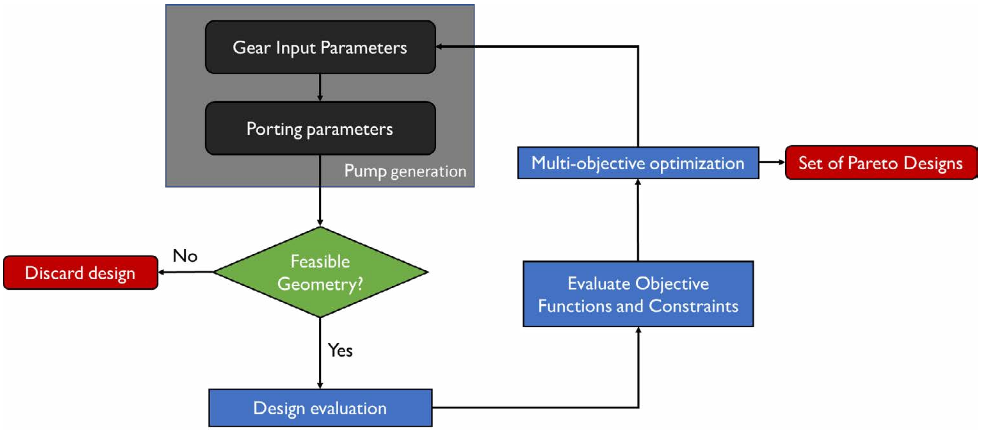

Figure 7: Algorithm for the first analytical step of the optimization

5.1.2. *Flow ripple*

The kinematic flow of the gerotor is defined as the sum of the outlet flows from all the DC, equations (4.2) and (4.3) describe the delivery flow rate from each DC which is defined as q_i for the ith DC. Whenever any DC is closing the negative of the volume change of the DC is defined as the kinematic delivery flow rate and when the DC is opening the delivery from the chamber is zero. The total kinematic flow (Q) is the sum of the delivery from each DC as shown in equation (4.2) and the calculation is done assuming an incompressible fluid and no internal leakages within the pump geometry.

$$Q = \sum_i q_i \tag{4.2}$$

$$q_i = \begin{cases} -\frac{dV_i}{d\theta_i} & \frac{dV_i}{d\theta_i} < 0 \\ 0 & \frac{dV_i}{d\theta_i} > 0 \end{cases} \tag{4.3}$$

The flow pulsation and flow power are calculated and used as objectives to be minimized in the optimization, to improve flow pulsation performance and they are calculated as per equations (4.4), (4.5) and (4.6)

$$\bar{Q} = \frac{1}{N}\sum_{i=1}^{N} Q_i \tag{4.4}$$

$$Q_{peak} = \frac{Q_{max} - Q_{min}}{\bar{Q}} \tag{4.5}$$

$$OF2\text{:} \, minimize \; Q_{peak} \tag{4.6}$$

5.1.3. Tooth tip leakage

Tooth tip leakages are the most significant source of pump volumetric losses especially in this case where they dominate the leakage loss. To quantify the tooth-tip leakage for each design the tooth-tip leakage is calculated using the correlation provided by Rituraj et al [4] with the geometrical values obtained from the numerical discretization of the gearset. Here h is the tooth tip gap height and κ is the curvature of the tooth where the displacement chamber leakages are calculated.

$$Q_{tip} = \frac{m}{4\pi}\int_{\theta=\pi-\frac{2\pi}{m}}^{\theta=\pi+\frac{2\pi}{m}} h^{2.5}\kappa^{0.5} d\theta \tag{4.7}$$

$$OF3\text{:} \, minimize \; Q_{tip} \tag{4.8}$$

5.1.4. Adhesive wear

Due to the constant sliding contact that happens between gerotor teeth, quantification of wear experienced by the gerotor and optimizing the design for improved wear resisting performance is something that is important while designing a new gerotor profile. In this study the classical Archard wear model, expressed in Eq. (4.9), which states that the volume of worn material, W is proportional to the frictional work, where F is the contact force, S is the sliding distance, H is the material hardness, and K is an empirical wear coefficient. This model can be normalized with respect to operating pressure, face width, and material properties to yield a dimensionless wear rate as given in Eq. (4.10), where $\bar{F}$ and $\bar{S}$ represent normalized contact force and sliding speed, respectively, p is the operating pressure, and ω_i is the inner gear rotational speed. The normalized sliding speed can also be expressed in terms of the instantaneous velocities of the inner and outer gear contact points, v_i and v_o, and the unit tangent vector $\hat{t}$, as shown in Eq. (4.12) and the outer gear rotation speed ω_o is used to normalize the sliding velocity. The purpose of using the non-dimensional wear equation (4.10) is to express the tendency of wear irrespective of the material that is to be used for the pump. Equation (4.11) describes the formulation of the force with is calculated using the pressure difference and the projected areas of the gear teeth and is normalized with the pressure difference and gear width. This objective function aims to minimize the maximum normalized wear rate over one full rotation, as defined in Eq. (4.13). A more detailed formulation and discussion is present in previous work of Robison et al [5-6].

$$W = \frac{KFS}{H} \tag{4.9}$$

$$\bar{W} = \bar{F}\bar{S} \tag{4.10}$$

$$\bar{F} = \frac{F}{\Delta ph} = \frac{\Delta p\sqrt{\Omega_x^2 + \Omega_y^2}}{\Delta ph} \tag{4.11}$$

$$\bar{S} = \frac{|v_i \cdot \hat{t} - v_o \cdot \hat{t}|}{\omega_o} \tag{4.12}$$

$$OF4\text{: } minimize\left\{max\,\bar{W}(\theta_i),\ 0 \le \theta_i < \pi - \frac{2\pi}{m-1}\right\} \tag{4.13}$$

5.1.5. Contact stress

When force is transmitted between two curved surfaces, local elastic deformation occurs as the load is distributed over a finite contact region. This deformation generates both normal and shear stresses within the material, collectively referred to as contact stress. The maximum shear stress typically develops below the surface and alternates in sign across the contact plane, which may result in fatigue-induced surface damage such as pitting under repeated relative motion. In the case of a gerotor mechanism, the meshing teeth can be idealized using Hertzian contact theory as two cylinders in contact, with their radii corresponding to the local radii of curvature of the inner and outer gear flanks. The resulting peak contact pressure, p_0, is a key indicator of mechanical durability and can be normalized with respect to material properties and operating pressure as expressed in Eq. (4.14). In this formulation, E^* represents the combined modulus of elasticity defined in Eq. (4.15) as per [15], while κ_i and κ_o denote the curvatures of the inner and outer gear profiles at the point of contact. The Poisson's ratios of the respective gears, ν_i and ν_o, together with their elastic moduli E_i and E_o, determine E^*. The maximum value of p_0 observed over a full revolution is used as the objective function Eq. (4.16), further discussion can be found in earlier studies by Robison et al [5, 6].

$$\overline{p_0} = p_0\sqrt{\frac{\pi}{E^*\Delta p}} = \sqrt{\bar{F}|\kappa_i + \kappa_o|} \tag{4.14}$$

$$\frac{1}{E^*} = \frac{1-\nu_i^2}{E_i} + \frac{1-\nu_o^2}{E_o} \tag{4.15}$$

$$OF5\text{: } minimize\left\{max\,\overline{p_0}(\theta_i),\ 0 \le \theta_i < 2\pi + \frac{2\pi}{m-1}\right\} \tag{4.16}$$

5.1.6. Lateral gap leakage

Lateral gap leakages in gerotor pumps arise through the thin clearances between the rotor side faces and the pump casing or endplates. Each differential section of a tooth along its axial height can be modelled as a Poiseuille flow between parallel plates, where the pressure difference acts laterally across the tooth width as is illustrated in figure 8. Assuming constant gap height, viscosity, and pressure difference, the leakage flow can be obtained by integrating the Poiseuille equation over the lateral direction of the tooth for each of the inner and outer gears, leading to a total leakage for each tooth as per equation (4.17), a more detailed description of the equation can be found in [6].

$$\overline{Q_L} = \frac{3Q_L\mu}{2h_z^3\Delta p} = \int_{x_0}^{x_1} \frac{1}{l}\,dx \qquad (4.17)$$

Where h_z is the lateral gap height, μ is the fluid viscosity, and l is the lateral flow length at a particular section. This expression can be normalized by the pressure difference to emphasize the geometric and fluid property dependencies, showing that longer, narrower teeth permit greater lateral leakage, whereas higher viscosity or improved axial sealing reduces it. Thus, while lateral leakages can theoretically contribute to volumetric losses, they remain negligible in well-sealed pumps with appropriately controlled axial clearances.

$$OF6\!: minimize\ \overline{Q_{L,\iota}} + \overline{Q_{L,o}} \qquad (4.18)$$

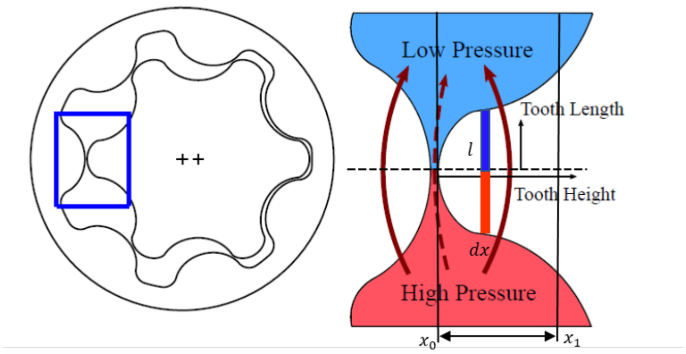

Figure 8: Representation of lateral gap leakage losses

5.2. Porting optimization

The porting optimization only has the objective to maximize the volumetric efficiency for every port angle of the design obtained from the multiple objective analytical optimization, multiple simulations were run where a lumped parameter based method was used to optimize the angular span of the porting considering the efficiency to be maximized in a manner similar to what is shown in figure 9 (a). The angular span of the porting geometry was parametrized as shown in figure 9 (b). To ensure the symmetric geometry for bidirectional operation of the pump the values of the four porting angles can be expressed with the parameters $\hat{\theta}_1$ and $\hat{\theta}_2$ as equations (4.19) and (4.20), while the volumetric efficiency was evaluated using equation (4.21) where Q_{sim} is the outflow predicted from the simulation in one revolution and V_{max}, V_{min} are the maximum and minimum values of the DCV that is predicted. For this study the parameters $\hat{\theta}_1$ and $\hat{\theta}_2$ were set to the range $\in [1, 2]$, while a 2D heat map could have been used to illustrate the performance variation of the pump with porting angle variation an optimizer which seeks the best combination was considered to be a better alternative. Also, all the simulations for the optimization are performed at a high pressure difference Δp of 100 bar and a shaft speed of 4000 RPM.

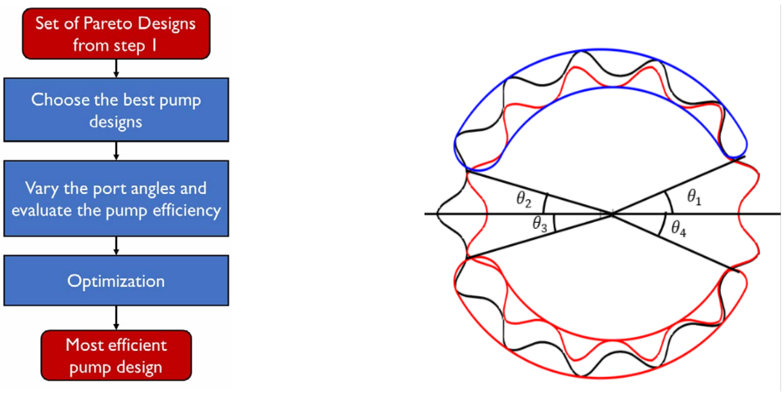

(a) (b)

Figure 9: (a) Algorithm for the second step of the optimization and (b) Representation of the angular parametrization of the porting.

$$\theta_1 = \theta_4 = \hat{\theta}_1 \cdot \frac{180}{m} \tag{4.19}$$

$$\theta_2 = \theta_3 = \hat{\theta}_2 \cdot \frac{180}{m} \tag{4.20}$$

$$\eta_{vol} = \frac{Q_{sim}}{mN \cdot (V_{max} - V_{min})} \tag{4.21}$$

6. RESULTS

For the first step optimization, a total of greater than 35000 designs were evaluated out of which there were around 2700 pareto designs. The resulting pareto fronts are plotted as shown in figure 10 and an industry pump whose specification are provided by the sponsor is used as a reference for the comparison of the performance, here the reference pump is represented as a red dot with a black outline to highlight it. In the pareto fronts shown in figure 10 while the pumps with the best leakage performance are chosen from the leakage pareto front. The leakage performance of the new profile is seen to be within the range of the reference profile, but this profile can be seen to have a big advantage particularly when it comes to the wear performance in which the chosen pareto designs have almost an order of magnitude better performance in comparison to the reference cycloidal design. Additionally, design clusters can be observed with respect to the leakage performance which can be attributed to the clusters of similar geometrical designs with small variations in parameters, the designs shown in figures 11 (a) and (b) are two such best performing designs from design clusters having low leakages.

The figure 11 (a) and (b) show the geometry of the pumps chosen with the best leakage characteristics while (c) and (d) shows the maps of the efficiency plotted against the angular span of the ports. While table 5 describes the geometric parameters chosen for each gear design. The best performing design out of which has an efficiency (η_{vol}) of 97.5%.

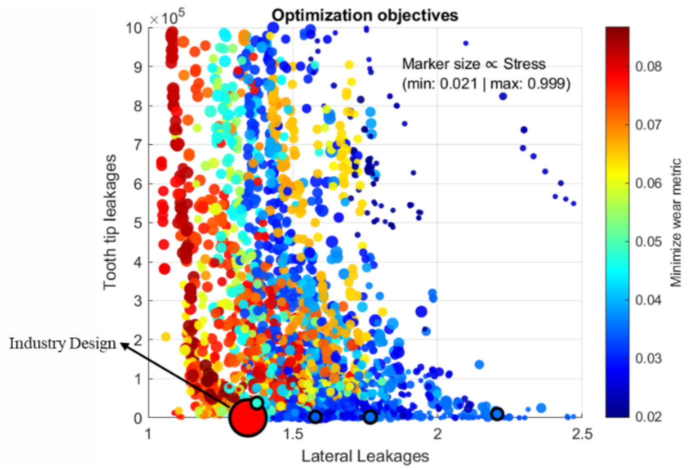

Figure 10: Pareto fronts from the analytical optimization

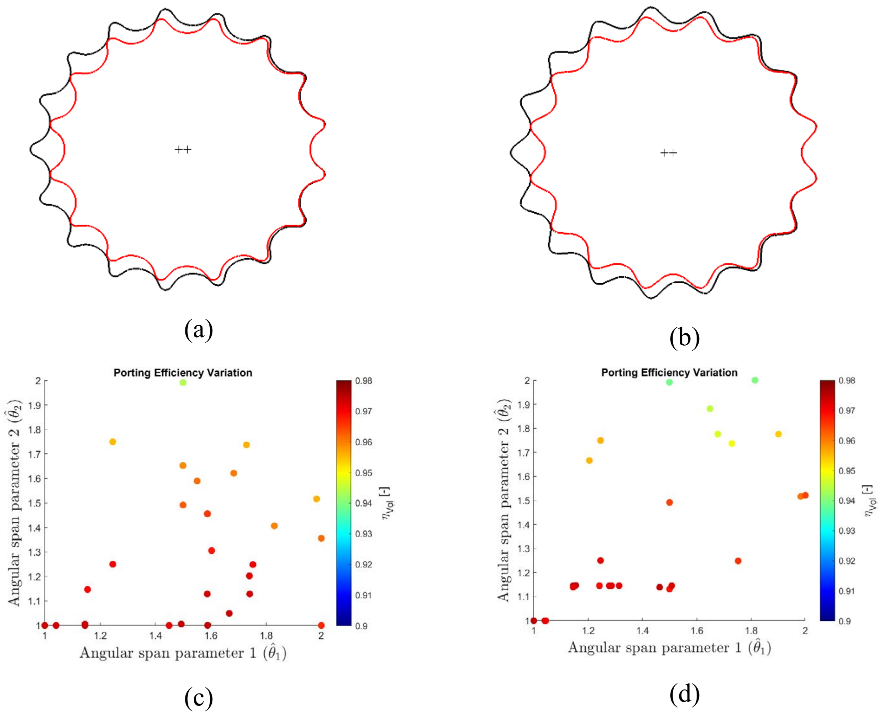

Figure 11: Results of the full simulation optimization for the ports.

Parameter	Value for (a)	Value for (b)	Unit
Number of Teeth	17	17	-
Eccentricity	2.623	3.085	mm
d	1.721	1.177	mm
b	0.977	1.599	mm
r_{po}	22.76	23.347	mm
s_{hypo}	7.955	9.493	mm
s_{epi}	1.977	0.064	mm
$\Delta\theta_1$.	346.33	343.18	deg
$\Delta\theta_2$.	288.45	264.60	deg

Table 5: Parametrization used to uniquely define the Kfloid gear in figures 11 (a) and (b).

7. CONCLUSIONS

A gear generation algorithm was developed to fully define the geometry, size, and other key parameters of a Kfloid-type gerotor pump. The Kfloid profile was subsequently optimized using modeFRONTIER in conjunction with Multics through a two-stage process aimed at maximizing volumetric efficiency for a specified delivery and pump size. A distinct Pareto front was established, and the optimized designs were compared with a reference industrial cycloidal type pump. The results indicate a modest improvement in volumetric efficiency, while the predicted trends suggest significantly better wear resistance and reduced flow ripple for the optimized Kfloid profiles. On comparing the resulting designs from the clusters that were formed as mentioned in section 6 we can see that design (a) has better lateral leakage performance compared to (b) due to the longer tooth geometry and on comparing the stress performance (b) performs better than (a) since geometry (b) has lower curvatures thus resulting in better stress performance.

Future work can focus on exploring mixed gerotor configurations with thinner teeth, similar to the Parafloid, Megafloid, and Geocloid profiles [6,7], with particular attention to hybrid geometries employing involute driving flanks due to their favourable drive characteristics [8].

8. ACKNOWLEDGEMENTS

The authors gratefully acknowledge ESTECO for providing access to the modeFRONTIER multi-objective optimization platform, which was used in this work to perform the numerical optimization studies.

9. NOMENCLATURE

Variable	**Definition**	**Unit**
m	Number of teeth of outer gear	-
e	Eccentricity	mm
d	Inner rolling circle radius	mm
b	Outer rolling circle radius	mm
r_{po}	Radius of outer gear base circle	mm
s_{hypo}	Shift in the hypocycloidal base radius	mm
s_{epi}	Shift in the epicycloidal base radius	mm
$\Delta\theta_1$.	Rotation of the rotating circle on the epitrochoid	deg
$\Delta\theta_2$.	Rotation of the rotating circle on the hypotrochoid	deg
L	Length of the connecting common tangent segment	mm
ν	Poissons ratio	-
E	Elastic modulus	MPa
$\hat{\theta}$	Porting span parameter for optimization	deg
κ	Curvature	mm^{-1}
H	Material Hardness	MPa
K	Empirical wear coefficient	$m^3/(Nm)$
S	Sliding distance	mm

10. REFERENCES

[1] Hill, M. F. (1927). Kinematics of Gerotors. The Peter Reilly Company, Philadelphia.

[2] Buckingham, E. (1949). Analytical Mechanics of Gears. Dover Publications, New York.

[3] Liu, H., & Lee, J.-C. (2017). Profile design and volumetric efficiency analysis of gerotor pumps for AWD vehicles. International Journal of Mechanical and Production Engineering, 5(4).

[4] Rituraj, F., & Vacca, A. (2020). An investigation of tooth tip leakages in gerotor pumps: modeling and experimental validation. Journal of Verification, Validation and Uncertainty Quantification, 5(1), 011001.

[5] Robison, A., & Vacca, A. (2018). Multi-objective optimization of circular-toothed gerotors for kinematics and wear by genetic algorithm. Mechanism and Machine Theory, 128, 150–168.

[6] Robison, A. J., & Vacca, A. (2021). Performance comparison of epitrochoidal, hypotrochoidal, and cycloidal gerotor gear profiles. Mechanism and Machine Theory, 158, 104228.
[7] Arinaga, S., et al. (2016). The latest trends in oil pump rotors for automobiles. SEI Technical Review, 82, 59–65.
[8] Choi, T. H., et al. (2012). Design of rotor for internal gear pump using cycloid and circular-arc curves. Journal of Mechanical Design, 011005.
[9] Jung, S. Y., Kim, M. S., Cho, H. Y., & Kim, C. (2009). Development of an automated design system for oil pumps with multiple profiles (circle, ellipse, and involute). Journal of the Korean Society for Precision Engineering, 26(3), 103–112.
[10] Nishida, Y., et al. (2018). Development of continuously variable discharge oil pump. SAE Technical Paper 2018-01-0932.
[11] Robison, A. J., & Vacca, A. (2020). Design of Asymmetric Gerotor Pumps. In International Scientific-Technical Conference on Hydraulic and Pneumatic Drives and Control (pp. 90-101). Cham: Springer International Publishing.
[12] Pareja-Corcho, J. C., Bartoň, M., Pedrera-Busselo, A., Mejia-Parra, D., Moreno, A., & Posada, J. (2024, August). On shape design and optimization of gerotor pumps. In Computer Graphics Forum (Vol. 43, No. 5, p. e15140).
[13] Jung, S. Y., Bae, J. H., Kim, M. S., & Kim, C. (2011). Development of a new gerotor for oil pumps with multiple profiles. International Journal of Precision Engineering and Manufacturing, 12(5), 835-841.
[14] Pellegri, M., Vacca, A., Devendran, R. S., Dautry, E., & Ginsberg, B. (2016). A Lumped parameter approach for gerotor pumps: Model formulation and experimental validation.
[15] Johnson, K. L. (1985). Contact Mechanics. Cambridge University Press.
[16] ESTECO. (2023). modeFRONTIER: Multidisciplinary Design Optimization and Process Integration Platform. ESTECO S.p.A., Trieste, Italy.
[17] Shah, K. Y., Cumberbatch, H., & Etchart, L. Optimization Techniques using modeFRONTIER-Process Review.